

REPORT DOCUMENTATION PAGE

*Form Approved
OMB No. 0704-0188*

The public reporting burden for this collection of information is estimated to average 1 hour per response, including the time for reviewing instructions, searching existing data sources, gathering and maintaining the data needed, and completing and reviewing the collection of information. Send comments regarding this burden estimate or any other aspect of this collection of information, including suggestions for reducing the burden, to Department of Defense, Washington Headquarters Services, Directorate for Information Operations and Reports (0704-0188), 1215 Jefferson Davis Highway, Suite 1204, Arlington, VA 22202-4302. Respondents should be aware that notwithstanding any other provision of law, no person shall be subject to any penalty for failing to comply with a collection of information if it does not display a currently valid OMB control number.

PLEASE DO NOT RETURN YOUR FORM TO THE ABOVE ADDRESS.

1. REPORT DATE (DD-MM-YYYY)	2. REPORT TYPE	3. DATES COVERED (From - To)
------------------------------------	-----------------------	-------------------------------------

4. TITLE AND SUBTITLE	5a. CONTRACT NUMBER
	5b. GRANT NUMBER
	5c. PROGRAM ELEMENT NUMBER

6. AUTHOR(S)	5d. PROJECT NUMBER
	5e. TASK NUMBER
	5f. WORK UNIT NUMBER

7. PERFORMING ORGANIZATION NAME(S) AND ADDRESS(ES)	8. PERFORMING ORGANIZATION REPORT NUMBER
---	---

9. SPONSORING/MONITORING AGENCY NAME(S) AND ADDRESS(ES)	10. SPONSOR/MONITOR'S ACRONYM(S)
	11. SPONSOR/MONITOR'S REPORT NUMBER(S)

12. DISTRIBUTION/AVAILABILITY STATEMENT

13. SUPPLEMENTARY NOTES

14. ABSTRACT

15. SUBJECT TERMS

16. SECURITY CLASSIFICATION OF:			17. LIMITATION OF ABSTRACT	18. NUMBER OF PAGES	19a. NAME OF RESPONSIBLE PERSON
a. REPORT	b. ABSTRACT	c. THIS PAGE			19b. TELEPHONE NUMBER (Include area code)

MEANS II: KNOWLEDGE ORIENTED MATERIALS ENGINEERING OF LAYERED THERMAL BARRIER SYSTEMS (NOMELT)

AFOSR Grant Nos:

**FA9550-05-1-0173, FA9550-05-1-0203,
FA9550-05-1-0229, FA9550-05-1-0039, FA9550-05-1-0163**

Kevin Hemker, Johns Hopkins University

Anthony Evans, University of California Santa Barbara

John Hutchinson, Harvard University

Tresa Pollock, University of Michigan

John Smith, Delphi Research Laboratory

David Srolovitz, Princeton University

Abstract

A team from academia, Air Force laboratories and industry has been assembled to develop a design code for one of the prevailing failure modes in thermal barrier systems used for aero-turbines. The failure mechanism to be addressed occurs in systems with two-phase bond coats and is manifest as abrupt delamination along the interface between the thermally grown oxide (TGO) and the intermetallic bond coat. The code will integrate several important time/cycle dependent phenomena, each with associated constituent models for: interface adhesion, bond coat deformation, sintering in the thermal barrier layer, etc. In this the second year of the project, efforts have focused on experimental characterization of the various layers and the development of hierarchical models, both of which are needed to characterize and define the salient governing phenomena. A previously developed interfacial delamination model is being adapted for this problem, and integration of these efforts will provide the pathway to the TBC design code.

Research Objectives

The main objective of NOMELT is to develop a code that facilitates the more aggressive design of multilayered thermal barrier systems. This code will incorporate the most important underlying micro-mechanical processes and permit industrial engineers to identify key material parameters and to probe the design space for improved systems. A hierarchical set of models is being developed to support the design code, which will predict the performance of a TBC subject to a single, dominant failure mechanism, as defined by the constituent models. The focus of this project is on a code for thermal barrier systems with two-phase bond coats that fail by delamination along the interface between the TGO and the bond coat. The constituent models developed for this purpose will address four specific time/cycle dependent phenomena: (i) evolution of the bond

coat, (ii) variations in the TGO, (iii) changes in the structure and properties of the ceramic top coat, and (iv) interfacial delamination.

The Integrated Materials Design Team

A team of academic, industrial and Air Force scientists and engineers has been assembled to undertake this project. The participants have extensive experience modeling materials behavior and conducting experiments at the variety of length-scales required to accurately describe multi-layered thermal barrier systems. The PIs (Hemker, Evans, Hutchinson, Pollock, Smith, Srolovitz) have a record of collaborating on projects involving multi-scale phenomena and have all contributed to the advancement of thermal barrier systems through mutual exchanges formulated at various international workshops on this topic. Our primary industrial contact has been Mike Maloney at Pratt & Whitney. Brian Tryon, who initially conducted research on this program at UM, and is now employed in the coatings group at Pratt and Whitney has also been a key contact for this program. This MEANS II program co-organized two international TBC workshops at UCSB in January of 2006 and January of 2007 with participation from the MEANS PI's, postdocs and students as well as industrial partners (primarily P&W and GE) and Air Force personnel.

Summary of the University of Michigan Effort

The focus of the University of Michigan effort was on (1) the evolution of the bond coat structure and properties during elevated temperature exposure under oxidizing conditions and (2) the development of a new apparatus for studying the failure process during cyclic oxidation of the MCrAlY class of coatings. Background and motivation for this research are first reviewed and a summary of results in the above two areas is given.

Background

Thermal barrier coating (TBC) systems provide gas turbine engine blades with the capability to operate at very high fractions of their melting temperature [1-4]. This ability to tolerate high temperature oxidizing atmospheres has been improved by the application of a metallic bond coat (BC) interlayer between the superalloy substrate and the thermally insulating ceramic top layer. The primary purpose of the BC layer is to provide environmental protection for the load-bearing superalloy substrate against oxidation and corrosion. In high temperature combustion environments, oxidation protection is achieved through formation of a thermally grown oxide (TGO) layer of α -Al₂O₃. While the TGO provides the coating system with an oxidation benefit, this thin interlayer may also endure large thermal and growth stresses that challenge the durability of the layered TBC system. Moreover, the BC structure evolves during high temperature exposure, potentially affecting the adhesion of TGO. Maintaining the mechanical integrity of the multi-layered thermal barrier structure during service presents a major challenge to advancing TBC technologies as these complex systems experience oxidation, interdiffusion, thermal expansion, and time dependent phase changes which introduce many life-limiting factors on the system [5-8].

Two main types of bond coat systems are commonly used: diffusion and overlay coatings. Diffusion coatings, such as B2 Pt-modified NiAl, are formed by electroplating a thin layer of Pt on the superalloy surface and aluminizing the structure typically by either chemical vapor deposition (CVD) [9] or pack cementation [10]. MCrAlYs (M = Ni, Co, NiCo, CoNi, or Fe) are the second type of commonly used BCs, often referred to as overlay coatings. An advantage of overlay coatings is that a specific composition can be placed on the superalloy surface without significant initial interdiffusion. Overlay coatings may be deposited by a large variety of methods, some of which include: low pressure plasma spray (LPPS), sputtering, air plasma spray (APS), and high velocity oxygen fuel (HVOF) thermal spray. In MCrAlY systems, the BC microstructure generally consists of B2 β (NiAl) and γ (Ni solid solution) phases, although γ' (Ni₃Al) and (Cr, Co) σ phases have additionally been shown to also exist [11, 12]. Various dopants (e.g. REs, Y, Hf, and Si) are regularly added to this type of BC to improve the oxidation behavior of the system.

Diffusion coatings such as Pt-aluminides typically fail due to ‘rumpling’ of the TGO which causes deformation of the ‘soft’ underlying BC, resulting in cracking along TGO interfaces [13, 14]. The failure mechanism in this MCrAlY system is less well understood because the TBC ceramic top layer coat often fails catastrophically by large scale delamination [15]. The dominant delamination mode has been reported as separation along the interface between the TGO and BC after isothermal or cyclic thermal exposures on samples with TBC top layer [15-17]. Because of the catastrophic character of the final failure, it is challenging to study the early stages of crack initiation and propagation in the MCrAlY systems. The relationship of failure events to the evolution of microstructures within the various layers of the coating system is also not well understood. While large geometric imperfections may induce crack initiation, the intrinsic features responsible for initiation of the failure are still not clear due to the extent of the delamination in conventional tests where specimens are uniformly heated. For this reason, a new localized heating experimental set-up was designed to explore the failure mechanism and microstructural evolution of the MCrAlY bond coats in the TBC systems without the complication of geometrical features such as sample edges. It is worth noting that catastrophic spalling of the TBC in blades often occurs near hot spots that develop due to the aero-thermal design of the blade and cooling passages. In order to eliminate the constraint effect of the ceramic top layer [18] and to directly observe the development of the TGO before failure, samples without the ceramic TBC top layer were used in this study. This study focuses on microstructural evolution and its influence on the failure initiation process within a NiCoCrAlY bond coat during cyclic oxidation.

Experimental Materials

Cylindrical samples (12mm in diameter and 105 mm in length) investigated in this study consisted of a ~100 μ m thick NiCoCrAlY bond coat (covering approximately 75 mm in length) deposited on a 2nd generation single crystal PWA1484 superalloy substrate. The NiCoCrAlY bond coat with nominal composition in Table 1 [19] was deposited by vacuum plasma spraying and subsequently shot peened and media-finished at Pratt and Whitney, USA. The microstructural characteristics of an as-coated specimen were

analyzed by scanning electron microscopy (SEM) combined with energy-dispersive spectroscopy (EDS), and electron microprobe analysis (EMPA).

Table 1. Alloy composition (wt. %) of the superalloy substrate (PWA 1484) [3] and the NiCoCrAlY bond coat (BC) [19].

Alloy	Ni	Co	Cr	Al	Ta	W	Mo	Re	Hf	Y	Si
PWA 1484	Bal.	10	5	5.6	8.7	6	2	3	0.01		
BC	Bal.	22	17	12.5					0.4	0.5	0.4

1. Bond coat evolution

Studies on bond coat evolution have examined the volume fractions and lattice parameters of the B2 and γ phases in the as-deposited condition and after annealing at 890°C, 950°C, 1000°C, 1050°C, 1100°C and 1150°C. Detailed microprobe studies have focused on the γ layer that forms just below the TGO, as delamination occurs along this interface. Additionally, characterization of the bond coat, in small pieces of airfoil from blades removed from service at the end of life, has been conducted.

Figure 1.1 compares the structure of the bond coat in the as-deposited condition with two blade sections that experienced lower temperatures/higher cycles and higher cycles/lower temperatures. With time during service it is apparent that Al is depleted from the bond coat, due to the formation of the Al_2O_3 TGO. As a result, the volume fraction of the B2 NiAl-based phase decreases, particularly within the upper 20 microns of the bond coat, and the Al content of the γ layer just beneath the TGO also decreases. The volume fraction of the B2 phase was measured to decrease as the exposure temperature increased.

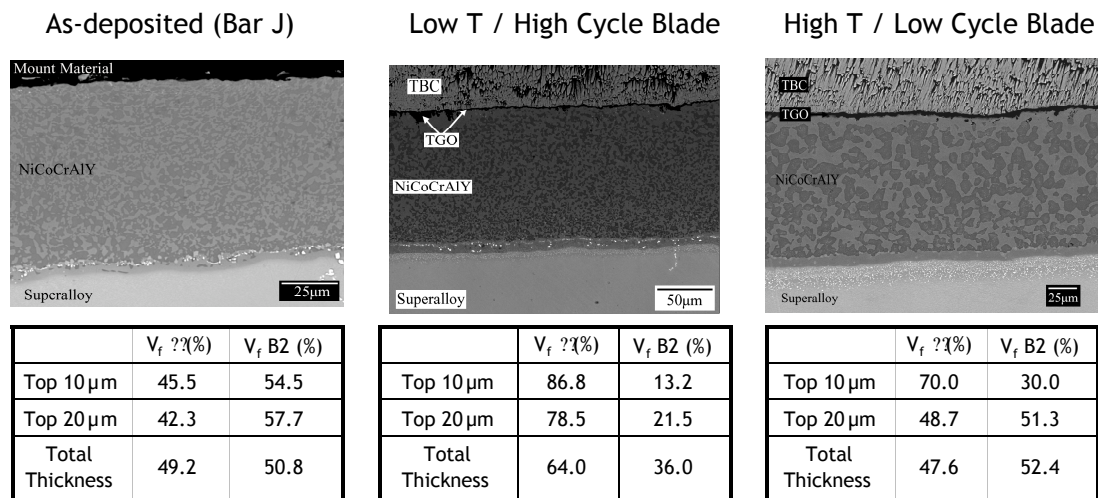


Fig 1.1: Comparison of initial coating structure and evolution of phases with cycling in two turbine airfoil samples.

TEM was used to characterize the microstructure of NiCoCrAlY bond coats at different stages of thermal cycling as well as bond coats that had seen service in commercial engine environments. Traditionally, NiCoCrAlY coatings are considered to consist of a NiAl based β -phase and Ni solid solution γ -phase. The latter however, contained fine, coherent precipitates of γ' (Ni_3Al) ~ 7 nm in size in the as-prepared bond coat and ~ 24 nm for the thermal cycled specimen (Figs. 1.2(a) and (b)). The unreasonably slow rates of coarsening suggests that γ' is not a stable, equilibrium phase at the peak thermal cycling temperature of 1100°C but rather forms during cooling.

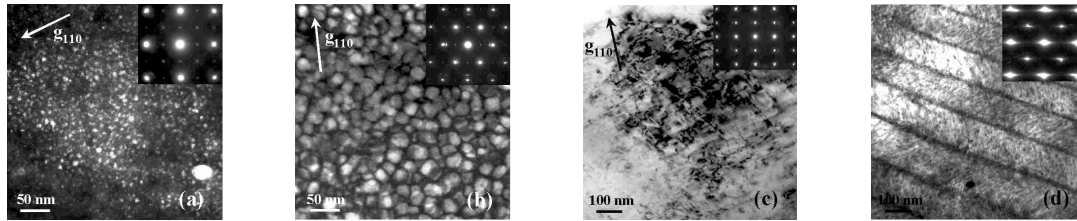


Fig. 1.2: Dark field images of γ' precipitates in the γ -phase of (a) the as-prepared bond coat and (b) thermal cycled bond coat. β -phase grains in the as-prepared bond coat (c) transform to martensite after thermal cycling (d).

In single-phase (Ni,Pt)Al bond coats superalloy-bond coat interdiffusion can lead to a martensitic transformation that has a critical effect on the failure mechanism of the TBC system. Fig. 1.2(d) shows that with thermal cycling the β -phase in the as-prepared NiCoCrAlY bond coat (Fig. 1.2(c)) also transforms to $L1_0$ martensite. TEM *in-situ* heating of the martensite revealed complete transformation to the β -phase at $\sim 100^\circ\text{-}140^\circ\text{C}$ while the reverse transformation took place at $\sim 50^\circ\text{-}80^\circ\text{C}$ on cooling. Therefore, although the strain produced by the volumetric change of the transformation is expected to be large the low transformation temperature together with the fact that NiCoCrAlY coatings are ‘two phase’ materials strongly indicate that martensite is not significant in this system.

TBC systems based on NiCoCrAlY bond coats typically fail by delamination at the thermally grown oxide (TGO)-bond coat interface. Sulfur impurities greatly reduce adherence and lead to premature oxide spallation. Reactive elements such as Y and Hf in the coating are thought to improve lifetime by forming stable sulfides and / or oxy-sulfides but direct evidence for this has been hard to come by. Using Scanning TEM (STEM) we have detected S precipitates within ‘pegs’ in a NiCoCrAlY bond coat that had seen service in a commercial engine (Fig. 1.3). The result highlights the role of reactive elements in getting the S before it reaches the TGO-bond coat interface and causes embrittlement.

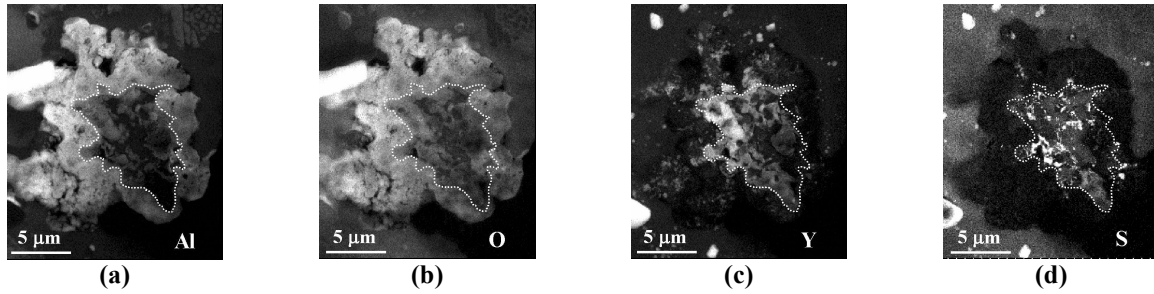


Fig. 1.3: STEM maps of (a) Al, (b) O, (c) Y and (d) S distribution within an oxide peg.

2. Design of a new thermal cycling test

Following cyclic oxidation, many TBC coatings fail by catastrophic spalling at the bond/coating TGO interface. While there must be flaws that enable a state of tension to develop in the TGO, the features responsible for initiation of the failure are still not well understood due to the character of the final failure. For this reason, UM has developed a new “hot spot” approach to cyclic oxidation. It is worth noting that catastrophic spalling of the TBC in blades often occurs near “hot spots” that develop due to the aero-thermal design of the blade and cooling passages.

The hot-spot apparatus cyclically heats cylindrical samples locally using a Lepel 2.5 kW, 130 kHz induction generator coupled to a plate concentrator coil. The concentrator coil was constructed with four turns of 5 mm diameter copper tubing with a base-plate thickness of 1.4 mm. The central hole in the concentrator plate was 15 mm in diameter, giving an air-gap of 1.5 mm between the concentrator plate and specimen periphery. At 130 kHz, the skin depth (the depth at which the strength of the magnetic field falls to $1/e = 0.3679$ of its surface value) in the BC plus the superalloy substrate is calculated to be about 2 mm [20, 21]. In contrast to other coil geometries, the magnetic field produced by the plate concentrator coil did not interfere with temperature measurements. The coil was positioned near the mid length of the coated region of the bar specimen, as shown in Figure 2.1. To maintain a constant temperature gradient during cyclic oxidation along the bar, the support base was water cooled while the opposite end of the sample was air cooled.

Cylindrical samples (12mm in diameter and 105 mm in length) investigated in the hot-spot apparatus in this study consisted of a $\sim 100 \mu\text{m}$ thick NiCoCrAlY bond coat (covering approximately 75 mm in length) deposited on a 2nd generation single crystal PWA1484 superalloy substrate. Cylindrical bar specimens were subjected to cyclic oxidation testing in the “hot spot” test apparatus in laboratory air at 1050 °C and 1100 °C. Samples were tested in as-media finished condition and with subsequent 600 grit polishing of the surface. Each cycle consisted of ramping to the maximum temperature in 10 minutes, followed by an isothermal dwell period of 45 minutes at 1050 °C before cooling to 400 °C in 10 minutes (Figure 2.2). Oxidation cycles were interrupted periodically (every 7 or 8 cycles) so the sample could be cooled to room temperature for inspection. To ensure that the specimens were heated uniformly around the periphery at the “hottest spot” region, K type thermocouples were securely located 60° apart around the specimen periphery at the

concentrator plate region. The bar specimens were centered in the coil so that the temperature difference between these six thermocouples was less than 5 °C. To measure the temperature gradients along the bar during each cycle, thermocouples were placed at different positions along the length of the bar; the measured temperature profile is shown in Figure 2.3. The thermocouple temperature measurements varied by less than 4% of the temperatures indicated by an optical pyrometer. To confirm that heating across the diameter of the bar was uniform for the heating rate utilized, the γ' volume fraction in the Ni-based superalloy substrate at the hottest spot region was carefully measured from periphery to center of the bar specimen after 51 cycles at 1050 °C. No obvious variation of the γ' volume fraction was observed across the sample and the measured results (51 ~ 54%, marked by the arrows in Figure 2.4) are consistent with the γ' volume fraction of the superalloy after heat treated at 1050 °C for 7.5 hours. Thus uniform heating across the bar sample was achieved during each oxidation cycle in the hot spot apparatus. For comparison, samples were also cycled in a conventional bottom loaded cyclic oxidation furnace utilizing a cycle that consisted of a 10 min ramp-up, 45 min dwell at maximum temperature, followed by a 10 min cooling cycle.

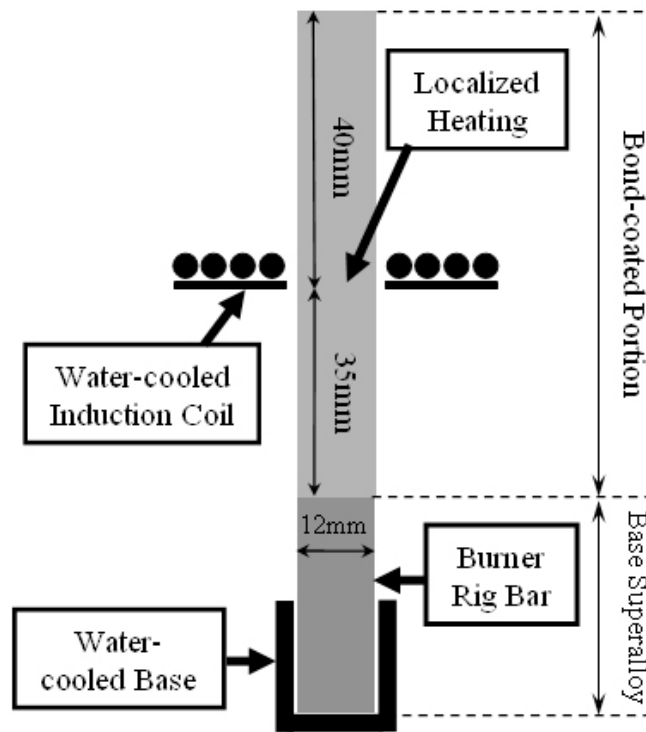


Figure 2.1. Schematic illustration of the “hot spot” test apparatus used in the cyclic oxidation testing.

Specimens were removed from testing when the first evidence of spallation was observed. The surface morphology of the sample was analyzed by optical, stereo, and scanning electron microscopy techniques. In order to prevent cracking or spallation of the oxide scale during cutting and subsequent polishing, an electroless nickel plating (10~20 mm in thickness) was applied on the surface of the oxidized sample. The sectioned pieces were mounted before polishing. The composition and the microstructure of cross-sections of the samples were examined by EMPA, SEM and EDS.

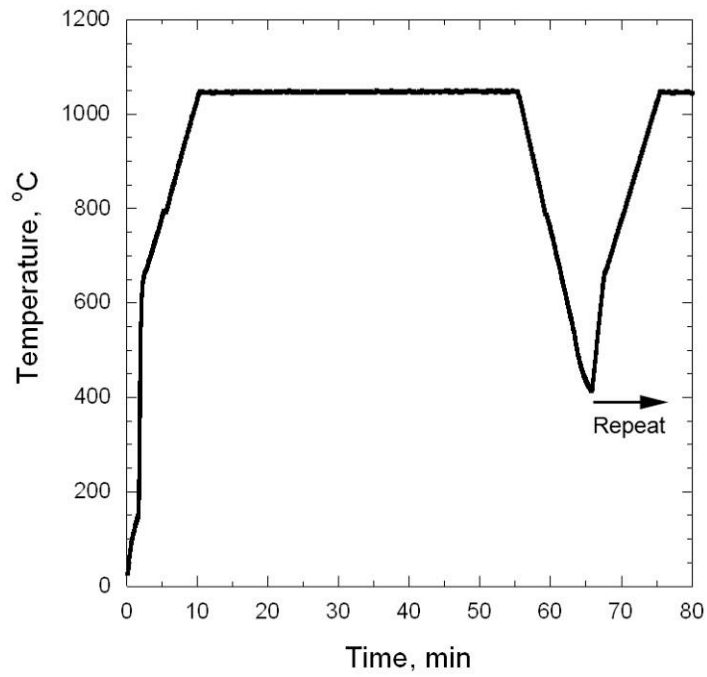


Figure 2.2. Measured temperature profile of the hottest spot region along the sample during one thermal cycle at 1050 °C.

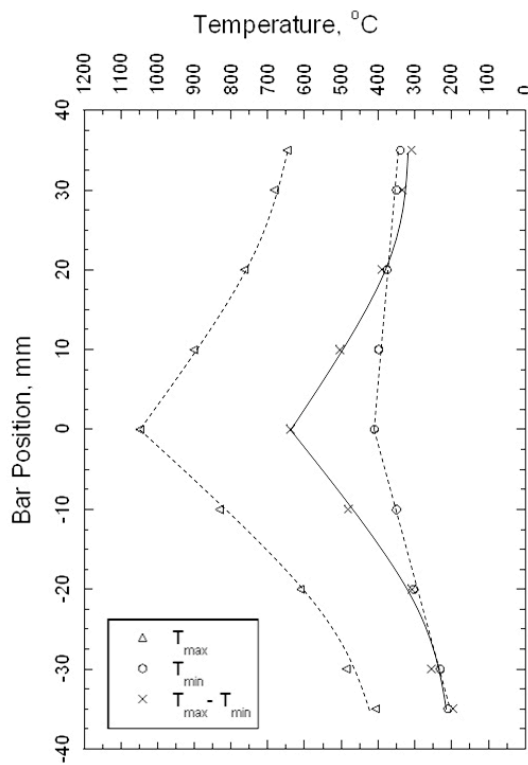
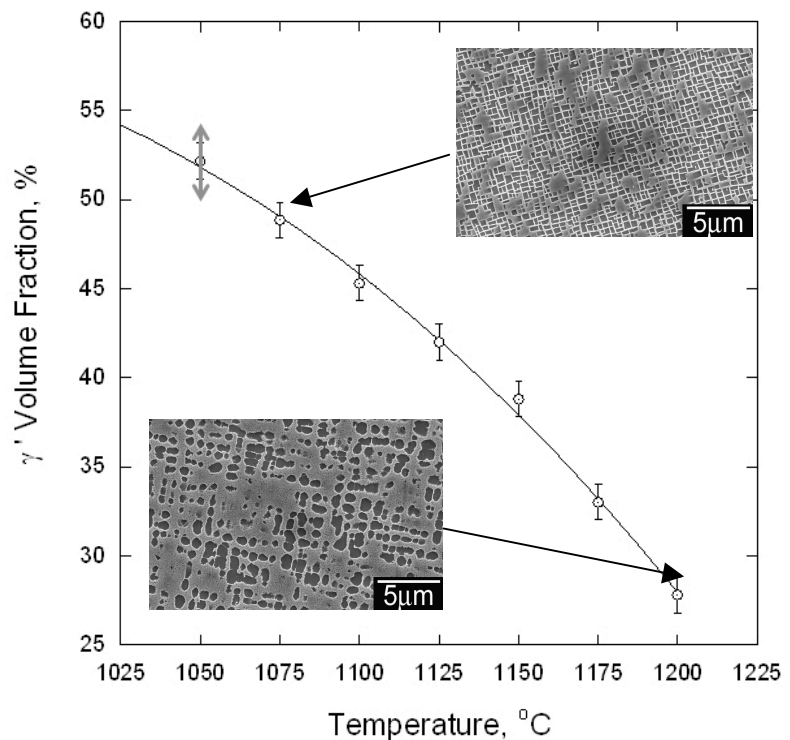


Figure 2.3. The measured maximum and minimum temperatures within one thermal cycle along the tested bar at 1050 °C.

The as-coated NiCoCrAlY bond coat thickness was $\sim 100 \mu\text{m}$ and was comprised of approximately equiaxed β NiAl (dark contrast) and γ (light contrast) phases, as shown in Figure 2.5a. The grain size of both phases was measured to be $2 \sim 3 \mu\text{m}$ in diameter. A small interdiffusion zone (IDZ) existed between the superalloy substrate and a slightly increased concentration of refractory elements at the BC/substrate interface was observed. The secondary electron (SE) image of the BC surface shows some surface roughness and the absence of well-defined grain boundaries (Figure 2.5b). Transmission electron microscopy (TEM) analysis of the as-coated NiCoCrAlY shows that the microstructure consists of three phases: β , γ , and fine γ' precipitates in the γ phase [12].

Figure 2.4. Temperature evolution of the γ' volume fraction and corresponding backscattered scanning electron (BSE) images in the superalloy substrate PWA 1484 after heat treatments for 7.5 hours. The two-head arrow marks the range of the measured γ' volume fraction in the superalloy substrate of a bar at the hottest region after 51 cycles at 1050°C .



Initial spallation of isolated regions of the TGO layer 120 to $500 \mu\text{m}$ in diameter around the hottest spot region of the bar sample was observed after 51 oxidation cycles at 1050°C (Figure 2.6a). EDS analysis confirmed that the irregularly shaped exposed areas bright in contrast were the NiCoCrAlY bond coat, indicating failure at the BC/TGO interface. Imprints of TGO grains in the exposed BC region and micro-cracks in the vicinity TGO layer were observed in the scanning electron micrographs, Figure 2.6(b). The failure surfaces also contained a significant density of embedded oxides that intrude into the bond coat due to preferential oxidation of the BC β phase, Fig 2.6(c). Similar local isolated spallation events were observed on specimens in the media finished and 600 grit polished conditions after cyclic oxidation in a traditional bottom loaded furnace after 149 cycles at 1100°C , Fig. 2.6(d). The density of spallation sites was somewhat lower in the media finished, compared to the polished samples. Similarly, these small-scale spallation events were also observed in the “hot-spot” test when cycling conducted with a maximum temperature of 1100°C .

Following observation of an isolated spallation event, the hot-spot sample subjected to cycling at 1050°C for 51 cycles was held in air with humidity level between 50% \sim 70% for 6

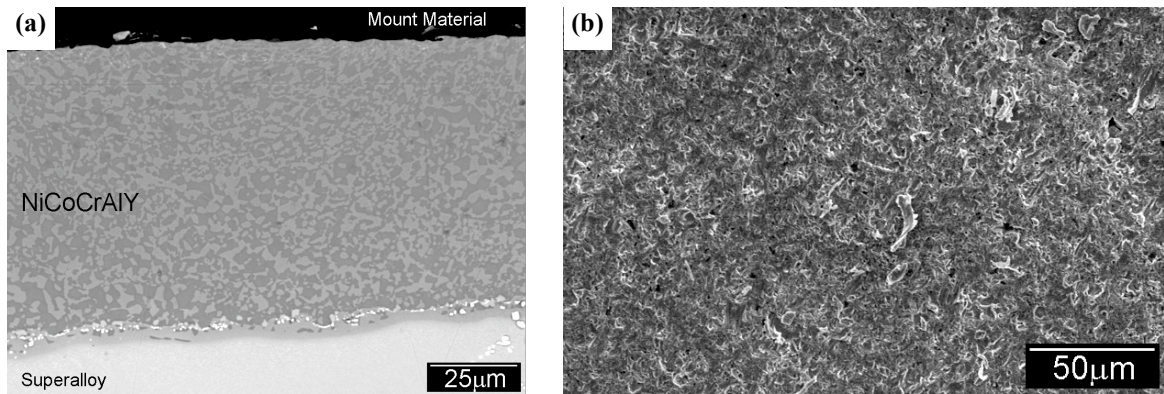


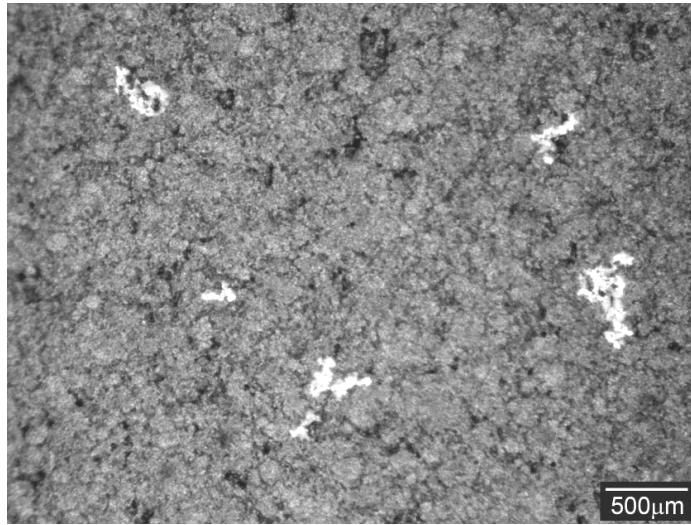
Figure 2.5. (a) BSE cross-section image of the as-coated NiCoCrAlY bond coating and (b) SE plan view image of the BC surface.

days. During this time, small-scale spallation events continued to occur in the “hot-spot” region of the sample, Figure 2.7(a). Finally, catastrophic spallation of the TGO at the hottest spot region then occurred during sectioning of the sample (Figure 2.7b). The backscattered scanning electron (BSE) image of the exposed bond coat surface (Figure 2.7c) reveals oxide domains remaining embedded in the bond coat. Most of embedded oxides have diameters between 2 and 10 μm , and some larger and interconnected domains of oxide with surface cracks (Figure 2.7c) were also observed. A high magnification SE image (Figure 2.7d) reveals imprints of the TGO grains in the exposed bond coats. Similar isolated spallation around the hottest spot region was observed on another bar after 62 oxidation cycles at 1050 $^{\circ}\text{C}$ and spontaneous, catastrophic spalling failure of the TGO at the hottest spot region then occurred during subsequent sectioning. No evidence of rumpling as a result of thermal cycling was observed in any of the cyclic oxidation experiments.

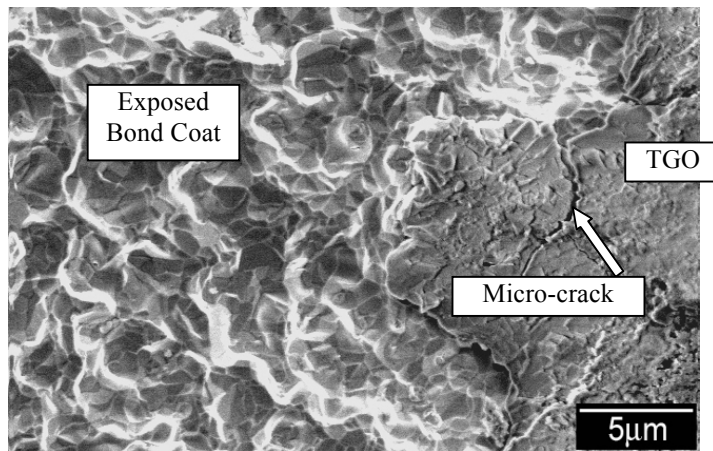
Figure 2.8 shows the cross-section microstructure of the sample at the “hottest spot” region after catastrophic spallation. Coarsening of the equiaxed γ and β grains in the BC to 5 ~ 6 μm in diameter was observed. The total BC thickness has increased to ~125 μm and due to Al depletion and dissolution of the β phase, a γ layer at both the TGO/bond coat and the BC/substrate interfaces formed. The average thickness of the top γ layer at the TGO/BC interface at the hottest spot region was 8.4 μm , which is close to the reported γ layer thickness on a MCrAlY BC with a top TBC layer after 100 h oxidation at 1100 $^{\circ}\text{C}$ [22]. The average TGO thickness at the hot-spot region was measured to be 2 ~3 μm . Morphological imperfections, i.e., “pegs” in the TGO developed, with localized internal oxidation at various points along the length of the BC. The distribution of the oxide intrusions appeared to be influenced to some degree by the size and morphological alignment of the original β grains in the bond coat.

Along the length of the specimen, the thickness of the total BC layer as well as the thickness of the two γ layers at the interfaces changes. As shown in Figure 2.9, the observed two γ layers formed at a maximum cycle temperature of 975 $^{\circ}\text{C}$ at both the TGO/BC and BC/substrate interfaces are thinner than the γ layers formed at 1005 $^{\circ}\text{C}$. Additionally, slightly decreasing in the size of the coarsened γ and β grains toward the lower temperatures was evident. Voids as marked in Figure 2.9 close to the BC/superalloy interface were observed as

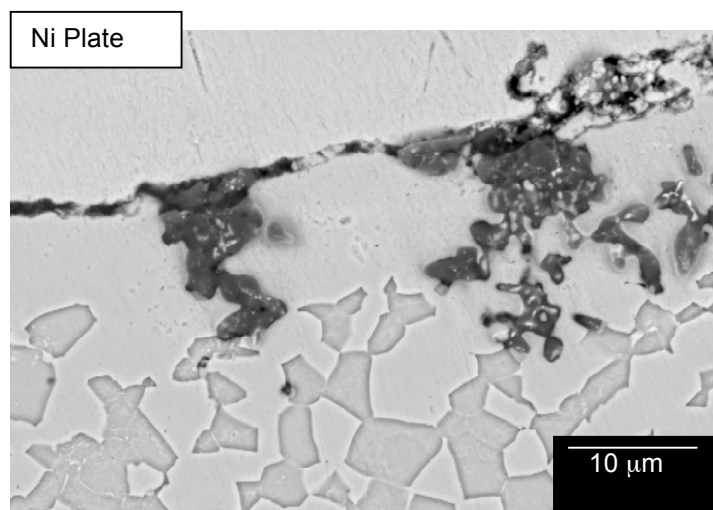
(a)

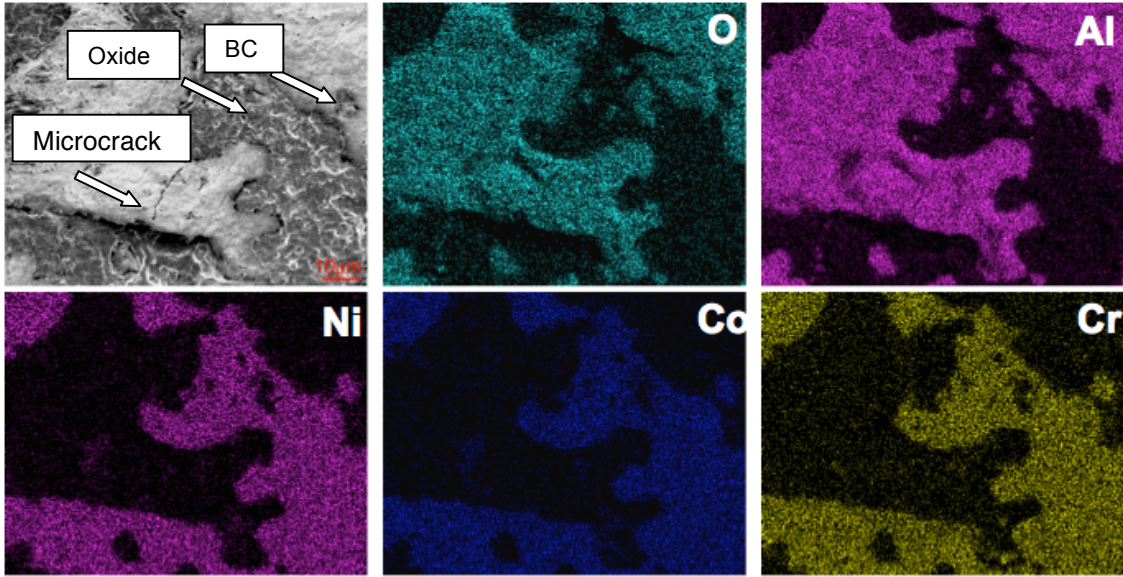


(b)



(c)





(d)

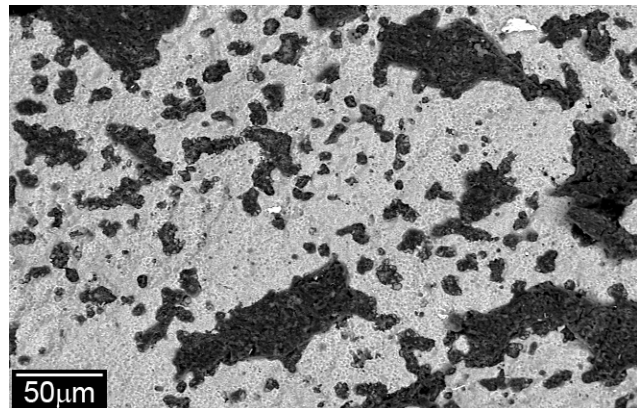
Figure 2.6. Top view of the TGO surface after initial spallation around the hottest spot region after 51 cycles at 1050 °C: (a) low magnification stereo optical microscopy image (b) high magnification SE image showing imprints of the TGO grains in the bond coat and micro-cracks in the TGO layer, (c) selective oxidation of the β phase and (d) spallation after conventional furnace cycle testing showing an oxide peg retained in a spalled region and an unoxidized BC fragment intersecting the oxide surface in an adherent region.

well. Moreover, pegs have been consistently observed on both sides of the hottest spot region of the bar specimen with lower temperatures, as long as a continuous TGO layer was formed. The size of the pegs varies from 5 μm up to 20 μm and larger pegs are more frequently observed at higher oxidation temperatures. The measured total thickness of the bond coat (from the top γ layer to the bottom IDZ) and the top γ layer as a function of temperature was plotted in Figure 2.10 and it decreases continuously with decreasing temperatures in the range of 1050 °C to 930 °C. The microstructure of the whole bond coat layer varies significantly with temperature. For example, there is a 20 μm change in thickness of the total bond coat at a temperature difference of 120 °C after 51 cycles. The overall volume fraction of the γ phase (including the two γ layers at the interfaces and the γ phase in the BC) measured by image analysis in the entire BC layer decreased from 58% to 47% from 1050°C to 930 °C after 51 cycles. The measured TGO thickness also decreases slightly from 2 ~ 3 μm to ~ 1.5 μm within this temperature range.

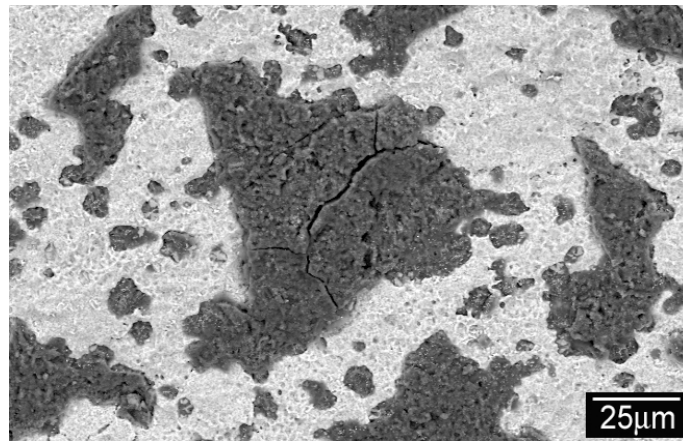
Within the pegs, the microstructure is not uniform and particles showing different contrast were observed at higher magnifications. The distribution of the elements within these pegs was examined by EDS element mapping. A series of typical element maps of a “peg” is shown in Figure 2.11. EDS analysis of the pegs revealed that these particles are rich in Y and slightly rich in Si and Hf, while the O contents are fairly uniformly distributed within the pegs. Y-rich domains within the γ layer were also observed, as highlighted in the ellipses, indicating inhomogeneous distribution of Y element within the bond coat after oxidation.



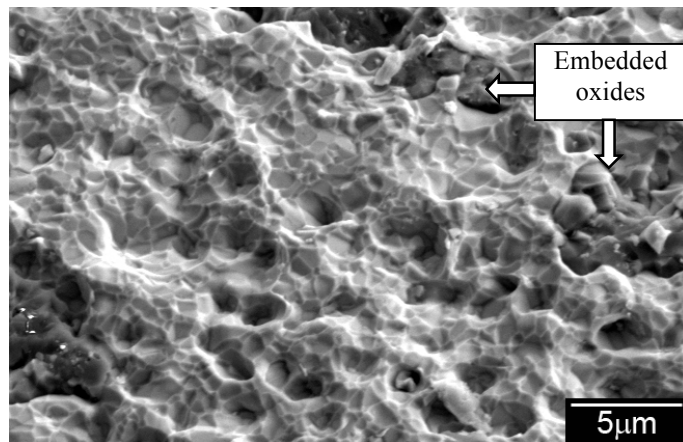
(a)



(b)



(c)



(d)

Figure 2.7. Top view of the bond coat surface after catastrophic spallation around the hottest spot region after 51 cycles at 1050 °C: (a) catastrophic spallation of the TGO at the hottest spot region, (b) and (c) low magnification BSE images, and (d) high magnification SE image showing imprints of the TGO grains in the bond coat.

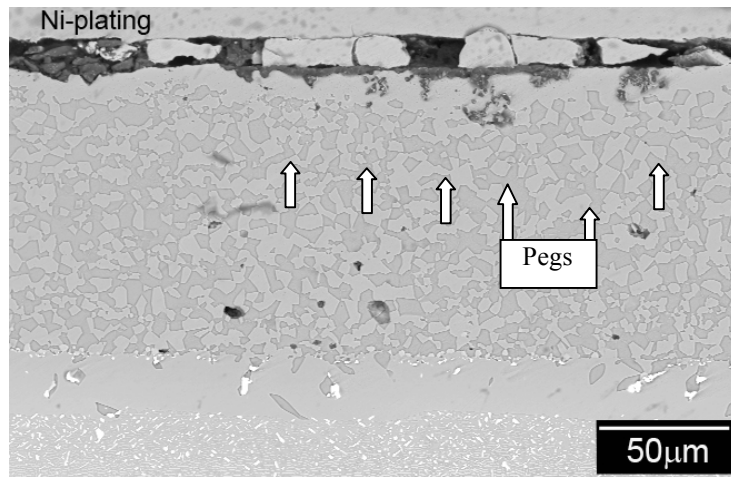


Figure 2.8. BSE cross-section image of the hottest spot region after catastrophic spallation, illustrating thickness heterogeneities or pegs of the TGO and formation of a γ layer at the TGO/BC and BC/substrate interfaces.

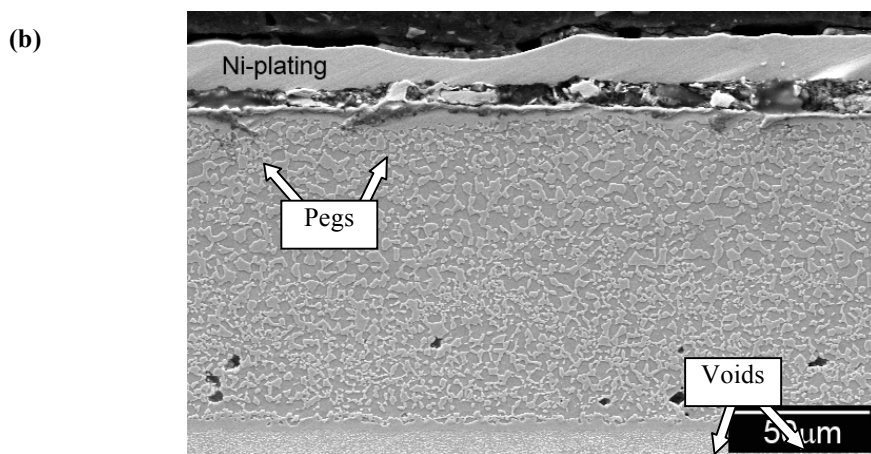
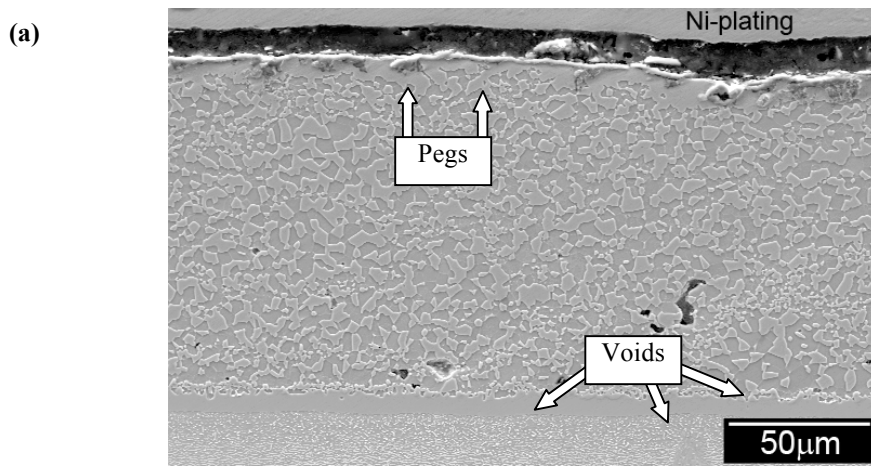


Figure 2.9. SE cross-section images of the regions off the "hottest spot" with maximum cycle temperature (a) 1005 °C and (b) 975 °C after 51 oxidation cycles.

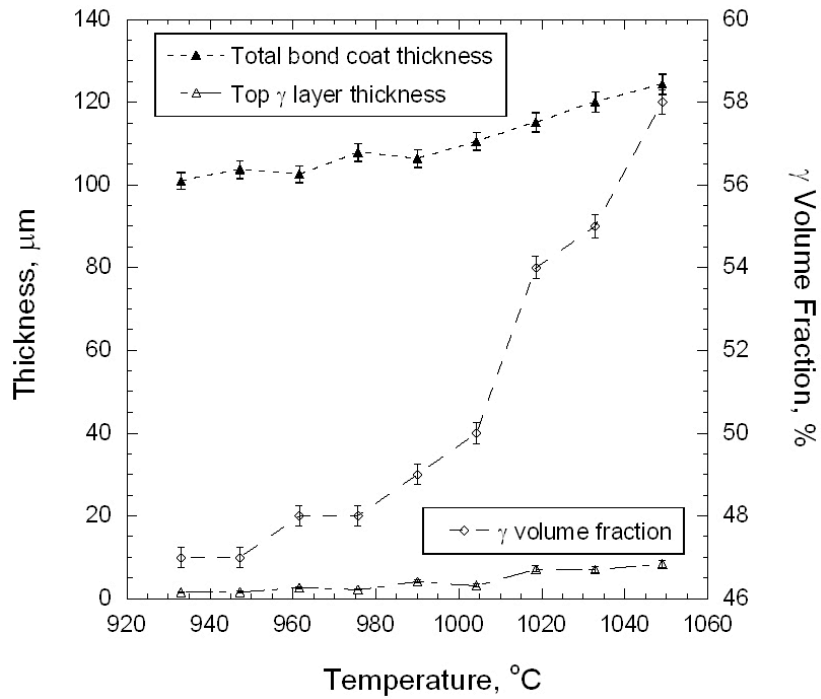


Figure 2.10. Measured thickness of the bond coat and the top γ layer, and the γ volume fraction in the bond coat plotted as a function of temperature after 51 oxidation cycles at 1050 °C.

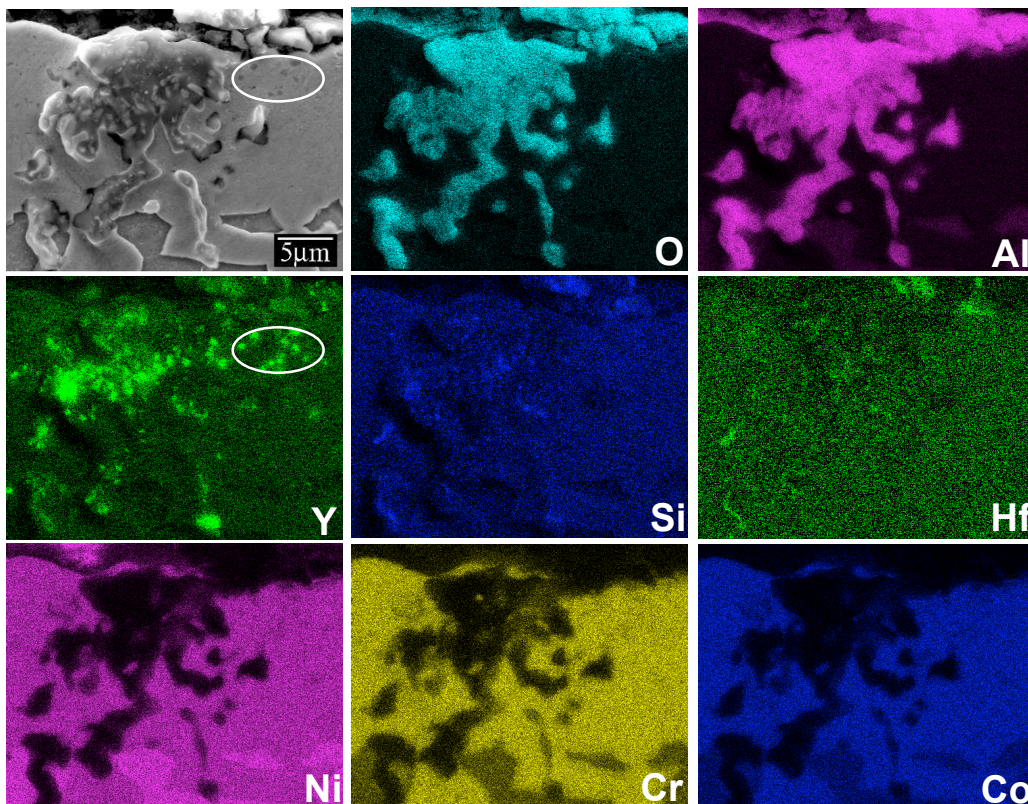


Figure 2.11. SE image and corresponding elemental maps of a “peg” in the top γ layer. Ellipses highlight inhomogeneous distribution of Y within the γ layer.

3. Discussion

Under the conditions investigated in this study, failure occurred in a localized manner at the BC/TGO interface. The failure surface contained a significant density of embedded oxides that extend into the bond coat due to preferential oxidation of the BC β phase. The remnant surface oxides at failure exhibited surface cracks indicative of a buckling delamination failure mode. The surface morphology of the initially spalled oxide scale with small fraction of exposed bond coat around the hottest spot region of the bar specimen (Figure 6a) appear similar to the bond coat surface exposed by wedge impression of a TBC coating with NiCoCrAlY BC after 10 h exposure at 1100 °C [14]. Depending on the amount of the stored strain energy in the TGO as well as the concentration and frequency of defects (transient oxides, TBC defects, reactive element-rich oxide protrusions, porosities, and surface defects), failure of the NiCoCrAlY systems can occur along either the TGO/TBC or the TGO/bond coat interfaces [24]. A weaker TBC/TGO interface fracture resistance compared to that of the TGO/BC interface was thus proposed by Mumm and Evans [22] at the early stage of oxidation when neither the strain energy nor the defects are significant. However, a detailed explanation was not given. Since the formation of the top γ layer is very sensitive to the oxidation period and temperature, a continuous γ layer may have not been formed after only 10 h of oxidation at 1100 °C of the TBCs. As a result, the interface toughness between the TGO and the bond coat with both γ and β phases contacting the TGO at the early stage of oxidation is higher than the interface between the TGO and the top γ layer in the later oxidation stages. Therefore, the delamination occurred along the TBC/TGO interface during the early stage of oxidation when a continuous γ top layer has not been formed, as observed in the indentation tests [24] and the wedge impression tests [22] of the TBCs. Low interface toughness between Al_2O_3 and Ni has been reported in the literature, especially when segregation of contaminants were present in combination with ambient moisture [25, 26]. Additionally, a substantial upturn of the thermal expansion coefficient (CTE) of the top γ layer at temperatures higher than 800 °C has been observed, compared to that of the as-deposited NiCoCrAlY bond coat in this study. Therefore, both the interface toughness and the thermal expansion mismatch between the TGO and the bond coat are indeed changing as the interface components change with extended oxidation. Detailed information regarding the CTEs within the NiCoCrAlY BC system and their effect on the failure of the TBCs will be reported elsewhere.

Isolated spallation of the TGO will occur when the stored strain energy in the TGO has reached a critical value. At this defects at the TGO/BC interface will act as crack initiation sites and cause localized spallation of the TGO [27]. Since the TGO/BC interface is fairly planar with few pores at the interface and no other defects present in the locally spalled regions, pegs are likely responsible for the initiation of failure. This is consistent with the high density of isolated, embedded oxides on spalled surfaces, such as shown in Fig. 2.7. Nucleation of separations around morphological imperfections in the TGO has also been indirectly observed by Mumm and Evans as well [22]. Prior fracture mechanics analyses [22] indicate that two criteria need to be satisfied for delamination failure of TGO on a superalloy substrate: a critical TGO thickness varies from 0.5 to 3 μm and a critical imperfection wavelength ranges from 20 to 100 μm [27]. These two requirements were likely satisfied for spallation of the TGO in this study since the TGO thickness 2 ~ 3 μm at the

hottest spot region and pegs with size up to 20 μm were exhibited on the hot-spot oxidized sample upon initial spallation. However, due to the difficulty in the subsequent sample preparation for selective cross-section cutting using focused ion beam instrumentation, further studies is needed to substantiate the initial spalled TGO regions in the NiCoCrAlY system.

Spontaneous catastrophic failure of the TGO layer with the largest thickness about 2 ~ 3 μm along the bar sample at the hottest spot region occurred after 6 days in air at room temperature or exposure to water during subsequent sectioning. This indicates that after a critical strain energy accumulated in the TGO, water vapor may influence interface crack growth, thus accelerating the final failure process. Catastrophic failure mediated by environmental-assisted subcritical crack growth along TGO / bond coat interface in a multilayered TBC system [29]. Janakiraman et al. proposed that the water vapor causes stress corrosion cracking at the Al_2O_3 interface based on the observation that water vapor caused the degradation rate to be increased by a factor of 2 when cracking and spalling present at the Al_2O_3 -CoCrAlY/superalloys interfaces [30]. Moisture enhanced crack growth has also been documented on the room-temperature time-dependent failure of a TBC on a MCrAlY BC [15]. These investigations are consistent with the fact that alumina/metal interfaces are prone to moisture enhanced subcritical crack growth [25, 31, 32].

The exposed bond coat surface with embedded TGO domains after catastrophic spallation (Figure 7a) in the present study is very similar to the failed bond coat surface of TBCs with plasma sprayed NiCoCrAlY BCs after cyclic oxidation [15, 16] and also similar to the exposed bond coat surface created by a wedge impression in TBCs with EB-PVD NiCoCrAlY BC after 100 h exposure at 1100 $^\circ\text{C}$ [22]. This indicates that release of the stored strain energy in the TGO is an important factor determining the spallation failure of the TGO, whether the constraint from the TBC ceramic layer exists or not. Imprints of the TGO grains and faceted morphology in the exposed bond coat surface have been observed by Mumm and Evans [22] as well, suggesting a relative brittle TGO/BC interface. Cracks have been observed in the TGO layer close to the initial spalled region (Figure 2.6b) and also in the large TGO domains embedded in the bond coat after catastrophic failure (Figure 2.7b). The morphology of the cracks exhibited buckling features, indicating that the TGO is in a compressive stress condition after cooling to room temperature.

A continuous γ layer was formed at the TGO/bond coat interface due to depletion of Al from the β phase during oxidation and also at the BC/substrate interface because of interdiffusion between the bond coat and the Ni-based superalloy substrate. Moreover, the thickness of these two γ layers changes continuously with changing maximum cycle temperatures (Figure 2.10). Therefore, the microstructure of the overall NiCoCrAlY BC layer strongly depends on the oxidation temperature as well as the number of thermal cycles. Additionally, the evolution of the microstructure of the NiCoCrAlY BC is also believed to strongly relate to the composition of the BC as well as the superalloy substrate since it has been reported that the rate of the β recession due to oxidation at the TGO/BC interface or interdiffusion at the BC/superalloy interface was significantly influenced by the Cr and Al concentration in the constitution [34, 36]. For the NiCoCrAlY system in this study, a 10% decrease of the maximum oxidation temperature results in 17% reduction in the total bond coat thickness and

a 13% decrease of the volume fraction of the γ phase after being cyclic oxidized for 51 cycles. Since the presence of the top γ layer with a certain thickness at the TGO/BC interface may significantly change the TGO/BC interface toughness, as discussed earlier, the relationship of the microstructure development of the NiCoCrAlY bond coat with temperature can provide insights and guidance on determining the oxidation pass of the catastrophically failed TBCs at the hot spot regions in real application, thus, is of great importance in understanding the failure mechanisms of the MCrAlY systems in turbine blades.

Morphological imperfections or pegs in the TGO as frequently exhibited in the TBC systems with MCrAlY bond coats [16, 17, 22, 24, 33, 38-40] have been consistently observed at the TGO/BC interface in the hot-spot tested specimens in this study. The size of the pegs varies roughly with oxidation temperature in this study and is believed to be sensitive to the bond coat composition, the deposition method and porosity, as well as its surface conditions [16, 17, 38]. Localized cracks confined to the regions around the pegs have been reported when spinels such as Ni/Co rich oxides were present in the pegs [16, 33, 38], though it is not certain yet whether these cracks are precursors of delamination. However, no cracks have been observed even at the largest pegs by Xu et al. when no spinels were present [17]. Since both spinels and cracks have not been found in the pegs in the NiCoCrAlY BC in this study (Figure 2.11), it might be possible that cracks tend to nucleate at the spinel regions in the TGO. However, further work is needed to prove this phenomenon.

EDS analysis of the pegs indicated that particles within the pegs are rich in Y and slightly rich in Si and Hf (Figure 2.11). Localized Y concentration enrichment in the TGO or the pegs has been observed by several authors [17, 22-24, 40]. EDS analysis in the TEM by Mercer and co-workers [40] revealed nano-scale oxides based on Y_2O_3 and HfO_2 inside the pegs. They further proposed that the likely phase of these oxide particles is a cubic fluorite of approximate composition $4HfO_2-Y_2O_3$ and the formation of these oxides is due to either the diffusion of Hf and Y from the bond coat or entrapment of nano-scale Hf- and Y-rich bond coat regions during TGO growth. Since inhomogeneous distribution of Y element in the top γ layer was observed after oxidation, as demonstrated in Figure 2.11, Y-rich domains are likely formed by a diffusion process when Al was depleted from the β phase during oxidation. It was reported that the formation of pegs was completely suppressed when a homogeneous Y distribution was achieved on a MCrAlY alloy with β precipitates smaller than 3 μm [39] or infusion of Pt into the bond coat surface was applied [38]. However, the size of the β phase will change with exposure temperature during oxidation, as observed in this study. Therefore, even the distribution of the reactive elements such as Y and Hf in the as-deposited bond coats is homogeneous, formation of the pegs in MCrAlY bond coats may still take place due to diffusion of the elements and the evolution of the BC microstructures during oxidation. An interesting experiment would be to then infuse the NiCoCrAlY bond coat surface with Pt to see if the formation of the pegs could be suppressed before failure.

References

1. R.L. Jones, *Thermal barrier coatings*, in *Metallurgical and ceramic protective coatings*, K.H. Stern, K.H. Stern. 1996, Chapman & Hall: London. pp. 194-235.
-

2. S.M. Meier and D.K. Gupta: *Journal of Engineering for Gas Turbines and Power, Transactions of the ASME*, 1994, vol. 116, p. 250-57.
 3. M.J. Stiger, N.M. Yanar, M.G. Topping, F.S. Pettit and G.H. Meier: *Zeitschrift fur Metallkunde*, 1999, vol. 90, p. 1069-78.
 4. A.G. Evans, D.R. Mumm, J.W. Hutchinson, G.H. Meier and F.S. Pettit: *Progress in Materials Science*, 2001, vol. 46, p. 505-53.
 5. N.R. Rebollo, M.Y. He, C.G. Levi and A.G. Evans: *Zeitschrift fuer Metallkunde/Materials Research and Advanced Techniques*, 2003, vol. 94, p. 171-79.
 6. J.A. Nychka, T. Xu, D.R. Clarke and A.G. Evans: *Acta Materialia*, 2004, vol. 52, p. 2561-68.
 7. D.R. Clarke: *Acta Materialia*, 2003, vol. 51, p. 1393-407.
 8. M.W. Chen, M.L. Glynn, R.T. Ott, T.C. Hufnagel and K.J. Hemker: *Acta Materialia*, 2003, vol. 51, p. 4279-94.
 9. K.S. Murphy: USA, Patent No. 5856027, 1999.
 10. G.W. Goward and D.H. Boone: *Oxidation of Metals*, 1971, vol. 3, p. 475-95.
 11. B. Baufeld and M. Schmucker: *Surface and Coatings Technology*, 2005, vol. 199, p. 49-56.
 12. B.G. Mendis, B. Tryon, T.M. Pollock and K.J. Hemker: *Surface and Coatings Technology*, 2006, vol. 201, p. 3918-25.
 13. V.K. Tolpygo and D.R. Clarke: *Acta Materialia*, 2000, vol. 48, p. 3283-93.
 14. D.R. Mumm, A.G. Evans and I.T. Spitsberg: *Acta Materialia*, 2001, vol. 49, p. 2329-40.
 15. S. Faulhaber, C. Mercer, M.-W. Moon, J.W. Hutchinson and A.G. Evans, *J. Mech. Phys. Solids* 54, 2006, 1004 - 1028.
 16. G.M. Kim, N.M. Yanar, E.N. Hewitt, F.S. Pettit and G.H. Meier: *Scripta Materialia*, 2002, vol. 46, p. 489-95.
 17. T. Xu, S. Faulhaber, C. Mercer, M. Maloney and A. Evans: *Acta Materialia*, 2004, vol. 52, p. 1439-50.
 18. S. Choi, J.W. Hutchinson and A.G. Evans: *Mechanics of materials*, 1999, vol. 31, p. 431-47.
 19. S.M. Meier, D.M. Nissley, K.D. Sheffler and T. A. Cruise: *International Gas Turbine and Aeroengine Congress and Exposition, Jun 3-6 1991*, Orlando, FL, USA, Publ by ASME, New York, NY, USA, 1991, pp. 7.
 20. M. Kush: *thesis*, University of Michigan, 1998, pp.
 21. B. Roebuck, D. Cox and R. Reed: *Scripta Materialia*, 2001, vol. 44, p. 917-21.
 22. D.R. Mumm and A.G. Evans: *Acta Materialia*, 2000, vol. 48, p. 1815-27.
 23. D. Strauss, G. Muller, G. Schumacher, V. Engelko, W. Stamm, D. Clemens and W.J. Quaddakers: *Surface & coatings technology*, 2001, vol. 135, p. 196-201.
 24. N.M. Yanar, F.S. Pettit and G.H. Meier: *Metallurgical and materials transactions A*, 2006, vol. 37A, p. 1563-80.
 25. A.G. Evans, J.W. Hutchinson and Y. Wei: *Acta Materialia*, 1999, vol. 47, p. 4093-113.
 26. D.A. Bonnell and J. Kiely: *Physica status solidi. A, Applied research*, 1998, vol. 166, p. 7-17.
 27. J.W. Hutchinson, M.Y. He and A.G. Evans: *Journal of the Mechanics and Physics of Solids*, 2000, vol. 48, p. 709-34.
 28. W.J. Brindley and R.A. Miller: *Surface & coatings technology*, 1990, vol. 43/44, p. 446-57.
 29. D.R. Clarke, R.J. Christensen and V.K. Tolpygo: *Surface and Coatings Technology*, 1997, vol. 94-95, p. 89-93.
 30. R. Janakiraman, G.H. Meier and F.S. Pettit: *Metallurgical and Materials Transactions A*, 1999, vol. 30, p. 2905-13.
 31. I.E. Reimanis, B.J. Dagleish and A.G. Evans: *Acta Materialia*, 1991, vol. 39, p. 3133-41.
 32. T.S. Oh, R.M. Cannon and R.O. Ritchie: *Journal of the American Ceramic Society*, 1987, vol. 70, p. C352-C55.
 33. Y.H. Sohn, J.H. Kim, E.H. Jordan and M. Gell: *Surface and Coatings Technology*, 2001, vol. 146-147, p. 70-78.
 34. J.A. Nesbitt and R.W. Heckel: *Metallurgical transactions A*, 1987, vol. 18, p. 2061-73.
 35. J.A. Nesbitt and R.W. Heckel: *Metallurgical and Materials Transactions A*, 1987, vol. 18, p. 2061-73.
 36. S.R. Levine: *Metallurgical and Materials Transactions A*, 1978, vol. 9, p. 1237-50.
 37. J.A. Nesbitt and R.W. Heckel: *Metallurgical transactions A*, 1987, vol. 18, p. 2087-94.
 38. N.M. Yanar, G.H. Meier and F.S. Pettit: *Scripta Materialia*, 2002, vol. 46, p. 325-30.
 39. T.J. Nijdam, C. Kwakernaak and W.G. Sloof: *Metallurgical and materials transactions A*, 2006, vol. 37A, p. 683-93.
-

40. C. Mercer, S. Faulhaber, N. Yao, K. McIlwrath and O. Fabrichnaya: *manuscript in preparation for publication*, 2008

Acknowledgment/Disclaimer

This work is sponsored by the Air Force Office of Scientific Research, USAF, under grants number FA9550-05-1-0173, 0203, 0229, 0039, 0163. The views and conclusions contained herein are those of the authors and should not be interpreted as necessarily representing the official policies or endorsements, either expressed or implied, of the Air Force Office of Scientific Research or the U.S. Government.

Personnel Supported

- Tresa Pollock, Professor, University of Michigan, Ann Harbor, MI
- Brian Tryon, Post-doctoral Fellow, University of Michigan, Ann Harbor, MI
- Fang Cao, Post-doctoral Fellow, University of Michigan, Ann Harbor, MI

Publications

- Microstructural observations of as-prepared and thermal cycled NiCoCrAlY bond coats, B. G. Mendis, B. Tryon, T. M. Pollock and K. J. Hemker, *Surface and Coatings Technology*, 201, 3918 – 3925, (2006).
- Microstructural Evolution and Failure Characteristics of a NiCoCrAlY Bond Coat in “Hot Spot” Cyclic Oxidation, F. Cao, B. Tryon, C.J. Torbet, *Acta Materialia*, submitted.
- High Temperature Properties of NiCoCrAlY Bond Coats, B.G. Mendis, C. Eberl, F. Cao T.M. Pollock and K.J. Hemker, *Metallurgical and Materials Transactions*, in preparation.

Transitions

- Dr. Brian Tryon, who worked on this project as a postdoc at the University of Michigan, has been hired by the Coatings group at Pratt & Whitney.

Awards Received

- Professor Pollock delivered the honorary China Distinguished Materials Scientist Lecture at the University of Science and Technology of Beijing in June 2008.
 - Pollock and her Ph.D. student Dr. Andrew Elliott received the AIME Rossiter W. Raymond Memorial Award for the Best Paper Among Journals in All Member Societies
 - Pollock delivered the Zay Jeffries Honorary Lecture for ASM International
-